Supporting Information

Mi et al. 10.1073/pnas.1501303112

SI Methods

Expression and Purification of Mouse–Human Chimeric BMP9. CHO cells stably expressed full-length pro-BMP9 containing the mouse prodomain and human GF domain. Cells were seeded in roller bottles in a 50:50 (vol/vol) mix of F12 and DMEM supplemented with nonessential amino acids, biotin, vitamin B_{12}, 0.2 μM methotrexate, and 10% (vol/vol) FBS and grown for 3–4 d to near confluence. Serum-containing growth medium was discarded, roller bottles were rinsed with PBS, and a serum-free production medium was added containing nonessential amino acids, 5 μg/mL insulin, 12.9 μM putrescine, 0.2 μM hydrocortisone, 29 nM selenium, and 0.6 g/L polyvinyl alcohol. Conditioned medium (CM) was collected at 48 h, and roller bottles were refed with fresh serum-free medium. Two sequential 48-h harvests were collected. CM was clarified by passing through a 5-μm pore filter (pass Profile) and a 0.22-μm pore Duropore filter (Millipore) (Patent: BMP9 Compositions WO 1995033830 A).

In a typical purification, the BMP9 procomplex was captured from ∼20 L of CHO CM by loading onto a 265-mL, 5.0 × 13.5-cm Q-Sepharose column equilibrated with 20 mM Tris, pH 8.6 (buffer A). After washing with 10 column volumes (CVs) of buffer A, BMP9 procomplex was eluted in a single step with buffer A containing 1.0 M NaCl.

To purify pro-BMP9, the main peak was exchanged into buffer A plus 30 mM NaCl with a 735-mL, 5.0 × 37.4-cm Sephadex G25 size-exclusion chromatography (SEC) column. The peak (720 mg total protein) was divided into thirds and loaded onto an 8-mL, 1.0 × 10.2-cm Source 15Q column equilibrated with 50 mM Mes, pH 6.1. After a 10-CV wash with equilibration buffer, the BMP9 procomplex was eluted with a 12-CV gradient of 0.03–1 M NaCl in 50 mM Mes, pH 6.1. SDS/PAGE and analytical SEC showed that pro-BMP9 eluted between 0.15 and 0.32 M NaCl. Pooled fractions from the Source15Q step (240 mg total protein from three runs) were further purified with three SECs on two tandem 2.15 × 60-cm TOSOH G3000SWL columns equilibrated with PBS (total CV = 435 mL). Pro-BMP9 and free BMP9 prodomain eluted in separate peaks as shown by SDS/PAGE and analytical SEC and were pooled separately, sterilized with a 0.22-μm syringe filter, and stored at 4 °C. Final yield was 125 mg (6.25 mg/L CM). Material was characterized by SDS/PAGE and N-terminal sequencing of individual Coomassie blue-stained bands. Present in the preparation was a putatively uncleaved prodomain GF precursor that yielded the N-terminal prodomain sequence, the prodomain that yielded a major sequence beginning with the N-terminal sequence and a minor sequence beginning at prodomain residue 46 (SLN), and a GF that yielded the GF sequence of SAG beginning at residue 298.

To purify mature BMP9, the main peak from the Q-Sepharose step of a separate purification run (720 mg total protein) was diluted with 19 volumes of 6 M urea, 25 mM Mes, and 25 mM Hepes, pH 6.5 and loaded onto a 265-mL, 5.0 × 13.5-cm Q-Sepharose column in tandem with a 15 mL, 1.6 × 7.5-cm SP-Sepharose column, both equilibrated with the same buffer. After washing with equilibration buffer, the columns were separated, and BMP9 was eluted from the SP-Sepharose column with a 12 CV gradient of 0–1 M NaCl in 6 M urea, 25 mM Mes, and 25 mM Hepes, pH 6.5. BMP9 eluted between 0.25 and 0.4 M NaCl. Fractions containing mature BMP9 were identified by SDS/PAGE and pooled. Protein (13.3 mg total) was further purified with two SECs on two tandem 2.15 × 60-cm TOSOH G3000SWL columns equilibrated with 6 M urea, 0.3 M NaCl, 25 mM Mes, and 25 mM Hepes, pH 6.5. Fractions containing mature BMP9 were identified by SDS/PAGE and pooled. Purified protein (11.4 mg) was concentrated on Amicon-ultra-15 centrifugal concentration devices and dialyzed into 5 mM NaCl, 10% (vol/vol) glycerol, 2.5% (wt/vol) glycine, and 5 mM glutamic acid, pH 4.5 centrifuged at 1,400 × *g*, sterilized with a 0.22-μm syringe filter, supplemented with 0.01% Tween-80, and stored at 4 °C. The final yield was 9.1 mg (0.46 mg/L CM).

For purification of the prodomain, pro-BMP9 in PBS was mixed with an equal volume of a 9:1 (vol/vol) solution of ethanol:1 M sodium acetate, pH 4.4. The mixture was incubated on ice for 1 h. Precipitated BMP9 prodomain was collected by centrifugation at 20,000 × *g* for 10 min and dissolved in 20 mM Tris, pH 8.0. BMP9 prodomain was further purified by ion exchange chromatography in the same buffer with a gradient of 0–1 M NaCl and S200 SEC.

Crystallization, Data Collection, and Structure Determination. For crystallization, pro-BMP9 in PBS was further purified by Superdex 200 HR SEC in 20 mM Bis-Tris-propane, pH 8.0, and 50 mM NaCl, and concentrated to 6 mg/mL. Screening using sparse-matrix, hanging drop vapor diffusion yielded a hit in 0.2 M zinc acetate, 0.1 M Mes, pH 6.0, and 15% (vol/vol) ethanol. Fine-matrix and additive screening found a final crystallization condition of 0.15 M zinc acetate, 0.1 M sodium cacodylate, pH 5.8, 4% (vol/vol) isopropanol, and 0.15 M nondetergent sulfobetaine (NDSB-211). Crystals were cryo-protected by rapid transfer to either 30% (vol/vol) ethanol (3.25-Å dataset) or 20% ethanol/10% glycerol (vol/vol) (3.3-Å dataset) in mother liquor and flash-frozen in liquid nitrogen.

X-ray diffraction data were collected at the Northeastern Collaborative Access Team beamline of Advanced Photon Source, Argonne, IL, and processed with X-ray Detector Software (1). For refinement of the 3.3-Å structure, eight datasets collected from eight isomorphic crystals were merged together. Initial phases were determined, and models were built using molecular replacement with single wavelength anomalous scattering, (2) using the BMP9 dimer (3) as a search model and weak zinc anomalous diffraction at 0.97918 Å in our 3.3-Å dataset. Subsequently, more accurate phases were solved using SAD in Phenix (2) with anomalous data collected at a zinc absorption peak at 1.2823 Å in a thin-sliced (0.2° oscillation per frame over 360° oscillation range), low-dose (1% transmission) mode using a PILATUS 6M detector. A total of 11 zinc binding sites were found by the program, and the electron density was well resolved, giving a figure of merit of 0.75. As the data for phasing and refinement are not isomorphic (Table S1), phases were transferred to the 3.3-Å dataset using density_cut in Phenix (2) and Molrep in CCP4 (4). Phases were extended to higher-resolution shells by solvent flattening and multicrystal averaging using the 3.3- and 3.6-Å datasets in Phenix (2). The 3.25-Å dataset was solved by molecular replacement using the structure from the 3.3-Å dataset.

Model building with Coot (5) and refinement with Phenix including phenix.rosetta_refine (2) were iterated many times. The resolution of the data was determined using paired refinement (6). In each asymmetric unit, there are two pro-BMP9 protomers, which form a functional dimer.

Superimposition. Arm domain superimposition was with pro-BMP9 residues 84–92, 107–115, 116–132, 143–155, 164–175, 177–197, and 226–237; pro-TGF-β1 residues 77–85, 101–109, 115–131, 135–147, 148–159, 164–184, and 224–235; and "super" in PyMol.

ELISA. BMP9 or pro-BMP9 was coated overnight at 4°C in PBS at 1 μg/mL on Nunc MediSorb 96-well plates. Plates were washed with PBST (PBS with the addition of 0.05% Tween 20) and blocked with 2% (wt/vol) BSA in PBST for 5–8 h at 20 °C. Blocking solutions were decanted, and receptor-Fc fusion proteins (R&D Systems, except ActRIIB-Fc, which was made in-house) were applied at 2 μg/mL and 1:3 serial dilutions in PBST with 2% (wt/vol) BSA and incubated at 4 °C overnight. Plates were washed three times with PBST, followed by the addition of JDC-10 mouse anti-human Fc conjugated with HRP (Southern Biotech) at 1:5,000 in PBST + 1% BSA. After overnight incubation at 4 °C, plates were washed with PBST (0.05% Tween 20), and color was developed with a standard 3,3′,5,5′ tetramethylbenzidine reagent. After stopping with 1 M H_2SO_4, plates were read at 450 nm. Binding data were plotted as the percentage of maximal receptor Fc bound in each experiment and fit to an equation for fractional saturation. Reported EC_{50} values represent the average and SD from triplicate experiments.

Pro-BMP7 Expression and Purification. HEK293 cells that stably express WT pro-BMP7 were kindly provided by Lynn Sakai, Shriners Hospital for Children, Portland, OR (7). Cells were cultured in DMEM with 10% (vol/vol) FBS and 0.5 mg/mL G418. Supernatants (2 L) were clarified by centrifugation, concentrated 10-fold with tangential flow filtration (Vivaflow 200; Sartorius Stedim), diluted 5-fold with Tris-buffered saline, pH 8.0 (TBS), and then concentrated 5-fold. The material was loaded onto 20 mL Ni-NTA agarose (Qiagen), washed with 200 mL of 1 M NaCl, 25 mM imidazole, and 20 mM Tris·HCl, pH 8.0, and eluted by 0.5 M NaCl and 1 M imidazole, pH 8.0. The Ni-NTA eluent containing pro-BMP7 was purified by SEC using a HiLoad 26/60 Superdex-200 prep grade column (GE Healthcare) in TBS. The pro-BMP7–containing fractions were pooled and further purified with a heparin Hitrap column (GE Healthcare), followed by Superdex S200 SEC in TBS. The peak fractions containing pure pro-BMP7 were pooled and concentrated using a 50-kDa cutoff centrifugal concentrator (Vivaspin) to 20 mg/mL, frozen in liquid nitrogen, and stored at −80 °C.

BMP9 Prodomain with a Coiled-Coil. A signal sequence, Strep-tag, His-tag, 3C protease cleavage site, and GCN4 coiled-coil were fused to the N terminus of the human BMP9 prodomain. The C-terminal Val-30 residue of GCN4 [numbering of Harbury et al. (8)] was mutated to cysteine. The construct in pEF1-puro was transiently transfected into HEK 293T cells (9). After culture for 3 d in Freestyle 293 medium, medium was concentrated, and buffer was exchanged with 20 mM Tris, pH 8.0, and 200 mM NaCl. Protein was purified by Strep-tactin affinity chromatography.

C2C12 Differentiation Assay. The C2C12 cell line was from American Type Culture Collection. p-Nitrophenyl phosphate was from Sigma-Aldrich. Activity of BMP9 was measured as previously described (10, 11) using induction of alkaline phosphatase, a biomarker of osteogenesis, in myoblast C2C12 cells. C2C12 cells seeded at 10^4 cells per well in 96-well plates 1 d previously in DMEM/10% (vol/vol) FBS were washed two times and suspended in 100 μL DMEM. Test proteins in 100 μL DMEM and 1 mg/mL BSA were added in triplicate. After 2 d, wells were washed with PBS, 50 μL distilled water was added, and plates were frozen and thawed three times. Freshly made 0.1 M glycine, pH 10.3, 0.1% Triton X-100, 19 mM p-nitrophenyl phosphate, and 17 mM $MgCl_2$ (50 μL) was added. After 30 min at 37 °C, 100 μL 0.2 N NaOH was added, and alkaline phosphatase activity was measured at 405 nm.

ITC. Proteins were dialyzed overnight against 0.5% sucrose, 5 mM NaCl, 0.01% Tween 80, 2.5% (wt/vol) glycine, and 5 mM glutamic acid, pH 4.5, degassed, and centrifuged at 20,000 × *g* for 10 min. ITC experiments used MicroCal iTC200 (GE Healthcare Life Sciences). Either 94.8 μM BMP9 prodomain was titrated into 5 μM BMP9 dimer in the cell or 47.4 μM BMP9 dimer was titrated into 10 μM BMP9 prodomain in the cell. A priming injection of 0.4 μL (not included in data analysis) was followed by 2-μL injections every 300 s. Data averaged over 2-s windows were analyzed using Origin 7. Fits using cooperative binding or two sequential binding sites did not yield markedly lower χ^2 values than a single-binding-site model, which was used to fit N (binding sites), K_a (association constant), and ΔH (enthalpy).

Negative-Stain EM. Pro-BMP9 and pro-BMP7 were purified by SEC using Superdex 200 HR preequilibrated with 20 mM Tris, pH 8.0, and 150 mM NaCl. The peak fraction was loaded onto glow-discharged carbon-coated grids, buffer was wicked off, and grids were immediately stained with 0.75% (wt/vol) uranyl formate. EM was as previously described (12). Images were recorded with a CCD camera at 52,000× magnification with a defocus of −1.5 μm. The pixel size was 2.88 Å at specimen level. Particles were interactively picked with BOXER in EMAN (13). Class averages were calculated with SPIDER (14) as previously described (12).

1. Kabsch WF (2001) Crystallography of biological macromolecules. *International Tables for Crystallography*, eds Rossmann MG, Arnold E (Kluwer Academic Publishers, Dordrecht), pp 730–734.
2. Adams PD, et al. (2010) PHENIX: a comprehensive Python-based system for macromolecular structure solution. *Acta Crystallogr D Biol Crystallogr* 66(Pt 2):213–221.
3. Brown MA, et al. (2005) Crystal structure of BMP-9 and functional interactions with pro-region and receptors. *J Biol Chem* 280(26):25111–25118.
4. Bailey S; Collaborative Computational Project, Number 4 (1994) The CCP4 suite: Programs for protein crystallography. *Acta Crystallogr D Biol Crystallogr* 50(Pt 5): 760–763.
5. Emsley P, Cowtan K (2004) Coot: model-building tools for molecular graphics. *Acta Crystallogr D Biol Crystallogr* 60(Pt 12 Pt 1):2126–2132.
6. Karplus PA, Diederichs K (2012) Linking crystallographic model and data quality. *Science* 336(6084):1030–1033.
7. Gregory KE, et al. (2005) The prodomain of BMP-7 targets the BMP-7 complex to the extracellular matrix. *J Biol Chem* 280(30):27970–27980.
8. Harbury PB, Zhang T, Kim PS, Alber T (1993) A switch between two-, three-, and four-stranded coiled coils in GCN4 leucine zipper mutants. *Science* 262(5138):1401–1407.
9. Mi LZ, et al. (2008) Functional and structural stability of the epidermal growth factor receptor in detergent micelles and phospholipid nanodiscs. *Biochemistry* 47(39): 10314–10323.
10. Partridge NC, et al. (1981) Functional properties of hormonally responsive cultured normal and malignant rat osteoblastic cells. *Endocrinology* 108(1):213–219.
11. Rosen V, et al. (1994) Responsiveness of clonal limb bud cell lines to bone morphogenetic protein 2 reveals a sequential relationship between cartilage and bone cell phenotypes. *J Bone Miner Res* 9(11):1759–1768.
12. Mi LZ, et al. (2011) Simultaneous visualization of the extracellular and cytoplasmic domains of the epidermal growth factor receptor. *Nat Struct Mol Biol* 18(9):984–989.
13. Ludtke SJ, Baldwin PR, Chiu W (1999) EMAN: semiautomated software for high-resolution single-particle reconstructions. *J Struct Biol* 128(1):82–97.
14. Frank J, et al. (1996) SPIDER and WEB: processing and visualization of images in 3D electron microscopy and related fields. *J Struct Biol* 116(1):190–199.

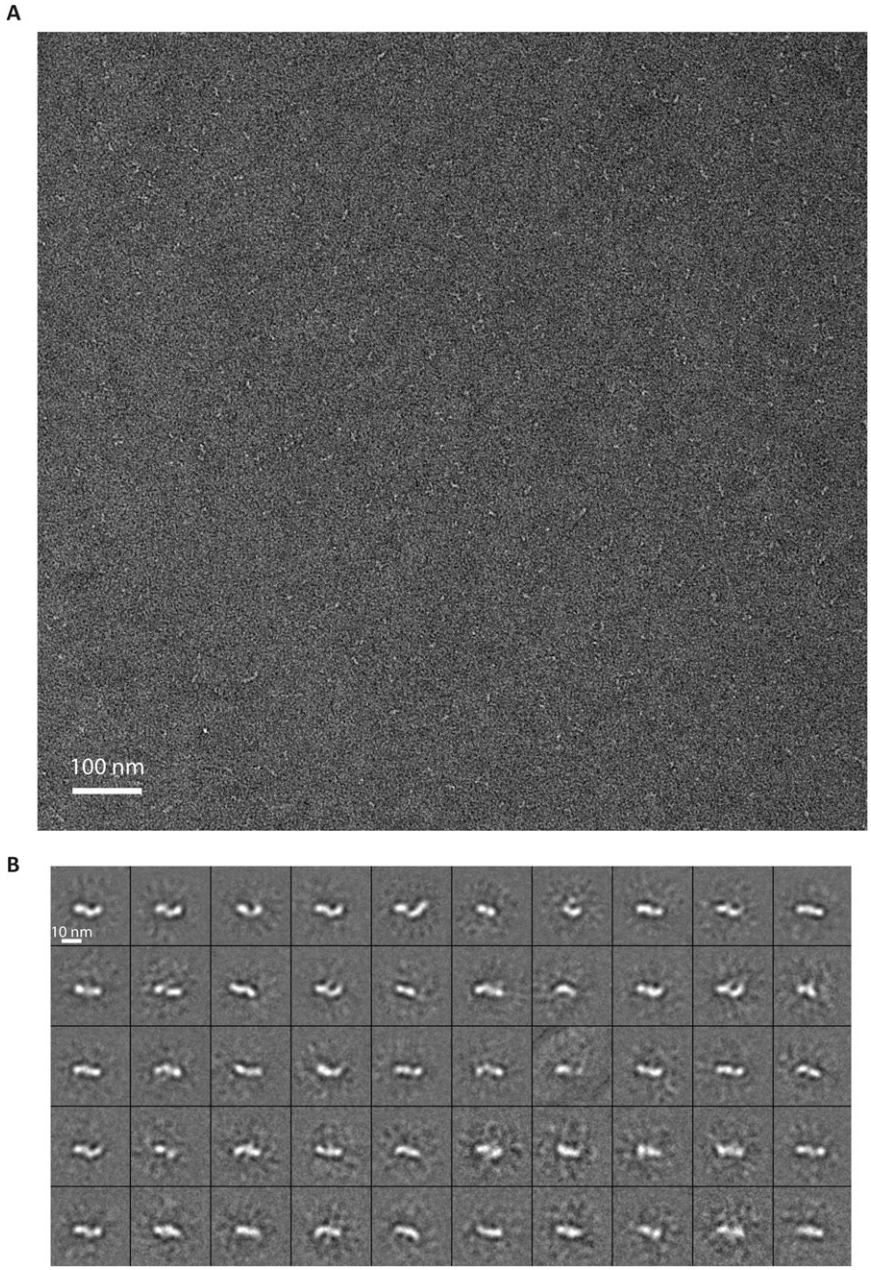

Fig. S1. Pro-BMP9 EM structure. Representative electron micrograph (*A*) and all 50 class averages of 7,098 particles (*B*). Averages are ranked (left to right in each row, from top to bottom row) by numbers of particles in each class.

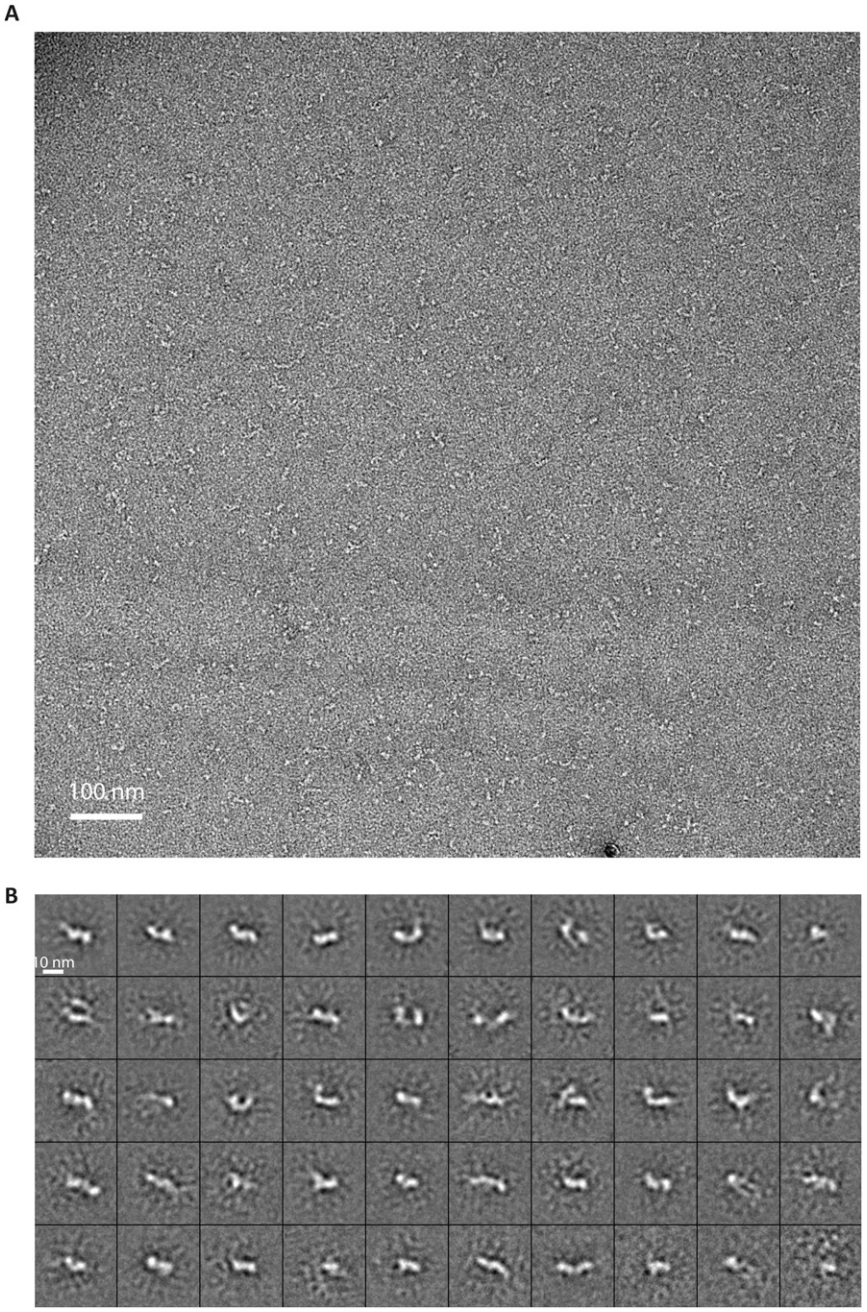

Fig. S2. Pro-BMP7 EM structure. Representative electron micrograph (*A*) and all 50 class averages of 4,427 particles (*B*). Averages are ranked (left to right in each row, from top to bottom row) by numbers of particles in each class.

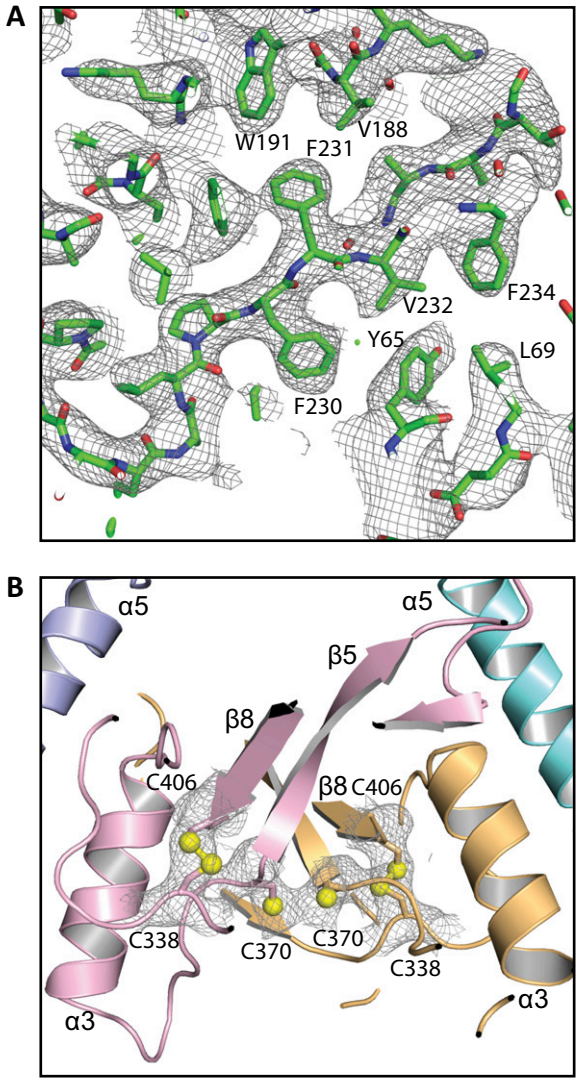

Fig. S3. Electron density map of pro-BMP9. (*A*) Representative region of experimentally phased electron density map of pro-BMP9 shown with mesh at 1σ contour level. (*B*) The free cysteines at the dimer interface and nearby disulfides shown with stick and S atom spheres, with experimentally phased electron density at 1σ level carved within 3 Å of cysteine residues. The structure appears to contain a mixture of disulfide and nondisulfide bonded Cys-370 residues at the GF monomer-monomer interface, consistent with presence of both GF monomers and dimers in nonreducing SDS/PAGE (Fig. S7 right, lane 2). In the refined molecular model, the disulfide is not built.

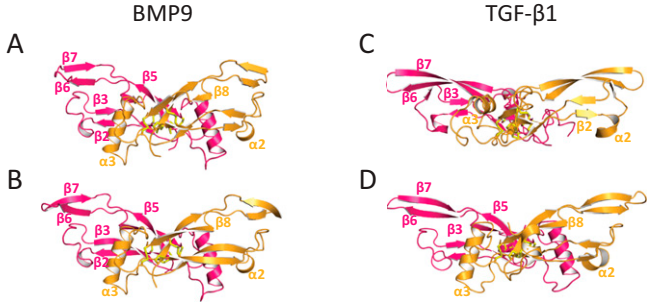

Fig. S4. Comparison of BMP9 and TGF-β1 structures in different complexes. (*A* and *B*) Comparison of prodomain-associated BMP9 (*A*) with receptor-bound BMP9 [Protein Data Bank (PDB) ID 4FAO] (*B*). (*C* and *D*) Comparison of prodomain-associated TGF-β1 (PDB ID 3RJR) (*C*) with receptor-bound TGF-β1 (PDB ID 3KFD) (*D*). The structures are represented in cartoon with one growth factor in pink and the other in gold.

Fig. S5. Alignment of human TGF-β family sequences including structurally aligned pro-TGF-β1 and pro-BMP9 sequences. Black dots mark decadal residues. Gold dots mark residues with >50% surface accessible surface area buried in prodomain-GF interfaces. Potential proprotein convertase cleavage sites and tolloid cleavage sites are marked with green and red circles, respectively. BMP8 shows BMP8A sequence which is almost identical to BMP8B.

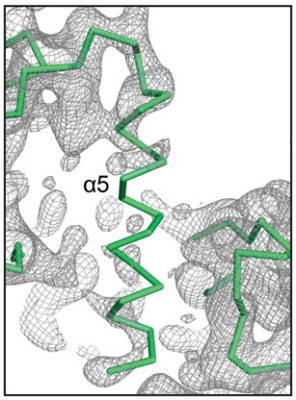

Fig. S6. Poor α5-helix density in one monomer of pro-BMP9 in the 3.25 Å dataset. Simulated annealing composite omit map is shown in mesh contoured at 1σ. The crystal was cryo-protected with 30% ethanol plus mother liquor.

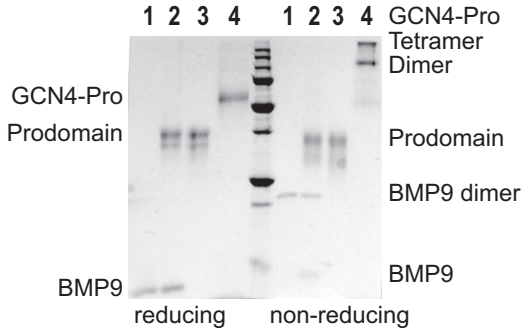

Fig. S7. Coomassie-stained SDS/PAGE of proteins used in crystallization and functional studies. Purified samples were loaded at equal molar amount: 1, BMP9; 2, pro-BMP9; 3, BMP9 prodomain; 4, GCN4-prodomain.

Table S1. Data collection and refinement statistics

	Zinc anomalous peak	Cryo with 20% ethanol/10% glycerol	Cryo with 30% ethanol
Wavelength (Å)	1.2823	0.97918	1.0332
Resolution range (Å)*	50.0–3.6 (3.69–3.60)	50.0–3.3 (3.39–3.30)	50.0–3.25 (3.33–3.25)
Space group	P 32 2 1	P 32 2 1	P 32 2 1
Unit cell a, b, c (Å)	121.9, 121.9, 223.6	120.8, 120.8, 220.6	120.3, 120.3, 221.3
α, β, γ (°)	90, 90, 120	90, 90, 120	90, 90, 120
Unique reflections*,†	31,412 (3,191)	29,933 (2,973)	29,711 (2,147)
Multiplicity*	14.5 (13.5)	23.3 (23.9)	4.03 (4.10)
Completeness (%)*	99.9 (99.9)	99.6 (100.0)	99.5 (99.7)
I/ σ(I)*	10.08 (0.43)	9.97 (0.67)	8.36 (0.53)
Wilson B-factor	136.5	142.7	128.2
R_{merge}*,‡	0.190 (4.82)	0.277 (5.26)	0.133 (3.394)
CC1/2 (%)*,§	0.999 (0.139)	0.994 (0.161)	0.995 (0.123)
Phasing and refinement			
Phasing FOM¶		0.75(0.29)	
Resolution range (Å)*		50.0–3.3 (3.36–3.30)	50.0–3.25 (3.35–3.25)
R_{work}/R_{free}*,‖		0.213/0.230 (0.335/0.314)	0.240/0.260 (0.387/0.384)
Nonhydrogen atoms			
Protein/NAG/Zn/water		4,802/56/10/21	4,681/42/10/14
RMSD bonds (Å)		0.002	0.002
RMSD angles (°)		0.59	0.62
Ramachandran plot**		93/7/0	93/7/0
(% favored/allowed/outliers)			
Clashscore**		3.03	5.06
Average B-factor		172.4	147.7
Macromolecules		171.8	147.2
Solvent		130.9	104.3
Protein databank codes		4YCG	4YCI

*Statistics for the highest-resolution shell are shown in parentheses.

†Friedel pairs are treated as separate reflections.

‡$R_{merge} = \sum_{hkl}\sum_{j}|\mathbf{I}_{hkl} - \mathbf{I}_{hkl}(J)|/\sum_{hkl}\sum_{j}|\mathbf{I}_{hkl}(J)|$, where $\mathbf{I}_{hkl}(J)$ and $\mathbf{I}_{hkl}$ are the jth and mean measurement of the intensity of reflection hkl.

§Pearson's correlation coefficient between average intensities of random half-data sets of the measurements for each unique reflection.

¶The value in parentheses is the figure of merit determined without solvent flattening and noncrystallographic symmetry averaging.

‖$R_{work} = \sum_{hkl}||\mathbf{F}_{obs}| - |\mathbf{F}_{calc}||/|\mathbf{F}_{obs}|$, where $\mathbf{F}_{obs}$ and $\mathbf{F}_{calc}$ are the observed and calculated structure factors, respectively. R_{free} is the cross-validation R factor computed for the 5% test set of unique reflections.

**Ramachandran and clash values were reported by Phenix.

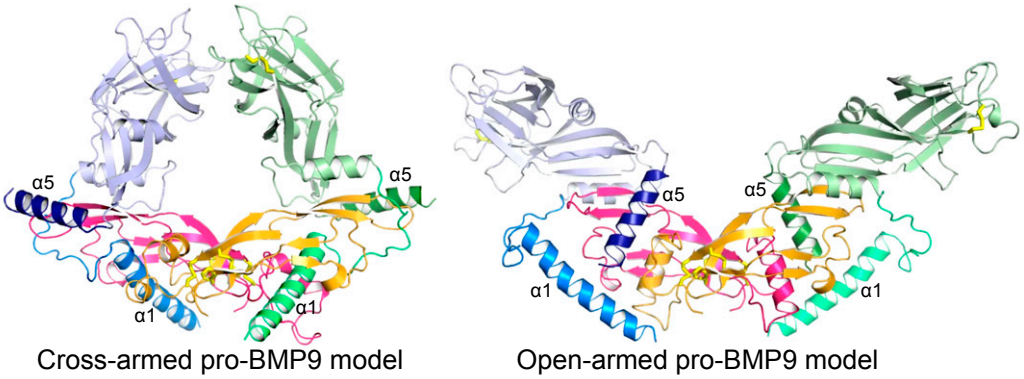

Movie S1. A feasible pathway for conformational change of pro-BMP9 between open-armed and cross-armed conformations. A cross-armed model of pro-BMP9 was constructed as described in *Discussion*. The movie, if looped, will display reversible conformational change from cross-armed to open-armed and open-armed to cross-armed. Structures are shown in cartoon with yellow disulfide bonds. BMP9 is shown with magenta and orange monomers. Prodomain monomers are shown in blue and green. Different shades are used for different elements. Thus for the prodomain monomer on the left, the arm domain and α2-helix are light blue, the α1-helix plus latency loop are marine, and the α5-helix is dark blue. The cross-armed pro-BMP9 model accommodates the longer α5-helix of pro-BMP9 in the same position as the shorter α5-helix of pro-TGF-β1. The open-armed pro-BMP9 model adds the α1-helix and the straight jacket elements to the pro-BMP9 crystal structure in positions where they do not clash. Using the open-armed and cross-armed models as starting and ending states, 88 morphing states in-between were calculated with adiabatic mapping using the script morph_dist from the Morph Server (1).

Movie S1

1. Krebs WG, Gerstein M (2000) The morph server: A standardized system for analyzing and visualizing macromolecular motions in a database framework. *Nucleic Acids Res* 28:1665–1675.